学位論文（要約）

First-principles calculations of the electronic structures

and optical absorption spectra of functional metal oxides

（機能性金属酸化物の第一原理電子状態計算及び吸光スペクトル）

平成２８年１２月博士（理学）申請

東京大学大学院理学系研究科

化学専攻

奈須　義総

Abstract

Our laboratory has reported functional metal oxides, e.g., epsilon iron oxide (ε-Fe_2O_3) exhibiting a large coercive field over 25 kOe and millimeter wave absorption property, and lambda titanium oxide (λ-Ti_3O_5) exhibiting external-stimuli-induced phase transitions at room temperature. In this work, to investigate the electronic structures and optical properties of functional metal oxides, first-principles calculations and optical measurements were conducted. The calculated electronic structure and the measured optical absorption spectrum of ε-Fe_2O_3 showed that ε-Fe_2O_3 has a wide band gap and exhibits light color. Furthermore, first-principles calculations and optical measurement of Al- and Ga-substituted epsilon iron oxides, ε-$Al_{0.5}Fe_{1.5}O_3$ and ε-$Ga_{0.5}Fe_{1.5}O_3$, were carried out. The obtained results showed that Al- and Ga-substitution enlarged the band gap and lightened the color of ε-Fe_2O_3.

The crystal structure of ε-Fe_2O_3, Al- and Ga-substituted epsilon iron oxides used in the periodic structure calculations, are orthorhombic in the *Pna*2_1 space group and have four cation sites (A–D site). A–C sites are octahedral sites, and D site is a tetrahedral site. In ε-Fe_2O_3, Fe^{3+} ions occupy A–D sites. For the calculations of ε-$Al_{0.5}Fe_{1.5}O_3$ and ε-$Ga_{0.5}Fe_{1.5}O_3$, the crystal structure with D site substituted by Al^{3+} or Ga^{3+} ions were used. First-principles calculations were conducted using Vienna *Ab initio* Simulation Package (VASP). The exchange-correlation functional was approximated with the generalized gradient approximation. The Hubbard U was taken into account in order to describe the Coulomb repulsion of Fe3d orbitals. $U-J$ value of 5 eV was selected. The basis set was regulated by a cutoff energy of 520 eV, and the k-mesh was set to 7×5×5.

Crystal structures were obtained by X-ray diffraction (XRD) and Rietveld

analyses. The magnetic properties were measured by superconducting quantum interference device magnetometer (SQUID). Optical spectra were measured by UV-vis spectrometer using highly dispersed polymer solutions of epsilon iron oxides, which were prepared by mixing the powder sample and an organic solvent containing polyurethane, polyvinyl chloride, toluene and methylethylketone.

First-principles calculations and optical measurement of ε-Fe$_2$O$_3$

Density of states of ε-Fe$_2$O$_3$ showed that O2p band is located below the Fermi energy (E_F) in the valence band, and Fe3d occupied band is located below the O2p band. Fe3d unoccupied band is located above the E_F. The band structure of ε-Fe$_2$O$_3$ suggested that ε-Fe$_2$O$_3$ has a band gap of 2.0 eV for down-spin transition and 2.4 eV for up-spin transition. By calculation of transition moments, this down-spin transition were assigned the transitions from the 4 top energy states in the valence band to the 6 bottom energy states in the conduction band. FeD site and neighboring O sites were mainly contributed to 4 top energy states in valence band, and FeC site was mainly contributed to 6 bottom energy states in conduction band. The calculated results well reproduced the observed spectrum. The observed optical spectrum showed that ε-Fe$_2$O$_3$ has a weak transition with a gap of 2.4 eV and a strong transition with a gap of 2.9 eV. These results indicated that ε-Fe$_2$O$_3$ exhibits a light color with a large band gap.

Al- and Ga- substitution effects on epsilon iron oxide for optical absorption

Fe^{3+} ions of ε-Fe$_2$O$_3$ can be substituted by Al^{3+} ions and Ga^{3+} ion, which Al^{3+} and Ga^{3+} ions selectively occupy the tetrahedral D sites. In this work, first-principles calculations and optical measurements of Al- and Ga-substituted epsilon iron oxides

were conducted.

Density of states of ε-Al$_{0.5}$Fe$_{1.5}$O$_3$ showed that O2p band is located below the E_F in the valence band, and Fe3d occupied band is located below the O2p band. Fe3d unoccupied band is located above the E_F. Al2p band and Al3d band are located below and above these bands, respectively. The band structure of ε-Al$_{0.5}$Fe$_{1.5}$O$_3$ indicated that this material has a band gap of 2.5 eV for down-spin transition and 2.6 eV for up-spin transition. The band gaps were enlarged from ε-Fe$_2$O$_3$ by Al-substitution. This enlargement can be explained as follows. Comparing the band structures of ε-Fe$_2$O$_3$ and ε-Al$_{0.5}$Fe$_{1.5}$O$_3$, 4 down-spin states of the valence band and 4 up-spin states of the conduction band near the E_F disappeared by Al-substitution of D site. This disappearance enlarged the band gap. The charge density maps showed that the down-spin state of valence band top is mainly contributed by D site. Optical spectrum of ε-Al$_{0.5}$Fe$_{1.5}$O$_3$ was calculated. Compared with the calculation result of ε-Fe$_2$O$_3$, the absorption peak of ε-Al$_{0.5}$Fe$_{1.5}$O$_3$ shifts to a higher energy by 0.1 eV, and the absorption is inhibited by half above 500 nm, which indicate that the present material has a higher transparency than ε-Fe$_2$O$_3$.

In order to confirm the calculation results, optical measurements of Al-substituted epsilon iron oxides, ε-Al$_x$Fe$_{2-x}$O$_3$ (x = 0.48, and 0.66), were conducted. XRD patterns and Rietveld analyses showed that these materials have an orthohombic structure with space group of $Pna2_1$, and Al^{3+} ions mainly occupied D site. The magnetic measurements showed a magnetic hysteresis loop at 300 K.

The UV-vis spectra of ε-Al$_x$Fe$_{2-x}$O$_3$ (x = 0.48, and 0.66) were measured. Absorption coefficients are lower than ε-Fe$_2$O$_3$. The observed spectra agree well with calculation results. Therefore, Al-substitution lightens the color of the ε-Fe$_2$O$_3$ based

magnet.

In addition, Ga-substitution effect was investigated using first-principles calculations and UV-vis spectrum. Ga-substitution also lighten ε-Fe_2O_3 with same mechanism as Al-substitution.

In this work, optical absorption of ε-Fe_2O_3 was investigated. First-principles calculations indicated that ε-Fe_2O_3 has a wide band gap and D site is mainly contributed to this transition. Furthermore, UV-vis spectrum of ε-Fe_2O_3 was measured. These results showed that this ferrite magnet exhibits high transparency. In addition, first-principles calculations of ε-$Al_{0.5}Fe_{1.5}O_3$ were carried out. The electronic structure was calculated by substituting Fe^{3+} ions of the tetrahedral D sites to Al^{3+} ions. The calculated results indicated that the band gaps were enlarged due to disappeareance of the energy states originated from teterahedral D site. Furthermore, UV-vis spectra of ε-$Al_xFe_{2-x}O_3$ (x = 0.48, and 0.66) were measured. The absorption coefficient were reduced by Al-substitution. Therefore, Al-substitution lightens the color of ε-Fe_2O_3. In addition, Ga-substitution also lighten the color of ε-Fe_2O_3 with the same mechanism as Al-subsitutuion.

Contents

Chapter 3. Al-substitution effect on epsilon iron oxide for optical absorption

Chapter 4. Ga-substitution effect on epsilon iron oxide for optical absorption

Chapter 1 Introduction

1.1. Functional metal oxides

Transition metal oxides consist of transition metal atoms and oxygen atoms. They exhibit various physical properties, such as metal-semiconductor phase transition and ferromagnetic-paramagnetic phase transition, and exhibits various colors from colorless to brilliant colors, derived from p, d electrons of the transition metal and/or p electrons of oxygen atoms [1-5]. Our laboratory has reported several functional metal oxides [6-12], e.g., epsilon iron oxide (ε-Fe_2O_3) exhibiting a large coercive field over 25 kOe and millimeter wave absorption property. In this study, I studied the color of epsilon iron oxide (ε-Fe_2O_3), which is one kind of ferrite.

1.2 Ferrite magnets

Iron oxides often exhibit ferromagnetism and typical iron oxides show deep color like red, dark brown, or black (Figure 1-1) [3-8, 13-18]. In this section, Fe_3O_4 and Fe_2O_3 are described in detail.

1.2.1 Fe_3O_4

Fe_3O_4, which is called magnetite, is obtained as natural mineral. Fe_3O_4 is known as the magnet used for the first time by mankind [3, 19]. The color of Fe_3O_4 is black. The crystal structure was reported in 1915, and it is the first mineral material to which X-ray crystal structure analysis was applied [20, 21]. The crystal structure is inverse spinel structure and the lattice constant is $a = 8.39$ Å. $Fe_3O_4 \times 8 = Fe_{24}O_{32}$ atoms are contained in the unit cell [22]. Fe_3O_4 contained divalent and trivalent Fe ion. The

charge states of Fe_3O_4 can be written as $Fe^{2+}_1 Fe^{3+}_2 O_4$, that is, one third of Fe ion have divalent charge states and two thirds of Fe ion have trivalent charge states. Fe_3O_4 has octahedral sites and tetragonal sites, and it can be written as Fe^{3+} [$Fe^{2+}Fe^{3+}$] O4. The inside of the bracket is an octahedral site and the outside of the bracket is a tetrahedral site. Fe^{2+} is contained only in the octahedral site, whereas Fe^{3+} is contained in both the octahedral site and the tetrahedral site.

Fe3O4 exhibits ferrimagnetism with a Curie temperature (T_C) of 850 K. In the inverse spinel crystal structure, the tetrahedral site is called A site and the octahedral site is called B site. Below T_C, the spins of A sites and those of B sites are antiparallel. The magnitudes of the magnetization of the two sites are different from each other, resulting in ferrimagnetism. In Fe_3O_4, transition appears in electrical conductivity and magnetic susceptibility around 120 K. This transition is called Verwey transition [23].

1.2.2 γ-Fe₂O₃

γ-Fe2O3 is called maghemite. The color of γ-Fe2O3 is brown or reddish brown. The crystal structure is very similar to magnetite. The difference is that all Fe ion of maghemite takes 3+ charge states. As a result of this difference, defects are included in a part of Fe sites. There are several reports on the crystal structure of γ-Fe2O3, depending on how defects are arranged (Figure 1-2) [24-28]. As the cubic crystal structure, the space group $Fd\overline{3}m$ and the lattice constant $a = b = c = 8.33$ Å is reported. In the case of this crystal structure, Fe3+ ions of 21 and 1/3, and lattice defect of 2 and 2/3 are contained. It is expressed by a composition of $Fe_8[Fe_{13.3}\square_{2.67}]O_{32}$, where the square ($\square$) represents defects. In this case, all tetrahedral sites are arranged by Fe^{3+} ion, however, Fe^{3+} and defects are randomly occupied in octahedral sites. On the other hand,

as a structure in which defects are ordered, a tetragonal space group has been reported, which the crystal structure is $P4_12_12$. In this case, the unit cells are three times as large as cubic structure along c axis, and the lattice constants are $a = 8.33$ Å and $c = 25.01$ Å.

γ-Fe_2O_3 exhibits ferrimagnetism at room temperature, and increasing the temperature causes transform to α-Fe_2O_3 at 700 - 800 K.

1.2.3 α-Fe_2O_3

α-Fe_2O_3 is called hematite. α-Fe_2O_3 shows red color as a feature and is widely used as red pigments. The crystal structure of α-Fe_2O_3 is a corundum structure of space group $R\bar{3}c$, hexagonal or rhombohedral crystal structure (Figure 1-3) [29-32]. The lattice constants of hexagonal crystal structure are $a = 5.034$ Å and $c = 13.75$ Å. All Fe sites are composed of octahedral sites.

α-Fe_2O_3 shows paramagnetic character above 956 K. On the other hand, below 956 K, α-Fe_2O_3 exhibits magnetism called weak ferromagnetism [33-36]. Furthermore, α-Fe_2O_3 shows phase transition at 260 K (called Morin temperature), and becomes antiferromagnetic state. Between 956 K and 260 K, the sublattice magnetization is not completely antiparallel. They tilt about 0.1 ° or less. Therefore, α-Fe_2O_3 exhibits weak ferromagnetism. On the other hand, below 260 K, this spin becomes completely antiparallel, so it becomes antiferromagnetism.

1.2.4 ε-Fe_2O_3

Epsilon iron oxide is found by Forestier et al. in 1934 and named as epsilon phase by Von R. Schrader et al. in 1963 [37, 38]. In 1998, the crystal structure was suggested by E. Tronc et al. At this time, the crystal structure was orthorhombic $Pna2_1$

with lattice parameter $a = 5.095$ Å, $b = 8.789$ Å, $c = 9.437$ Å (Figure 1-4) [39]. Fe^{3+} ion has four cation sites. FeA, FeB and FeC sites are octahedral sites, and FeD site is tetrahedral site. The formula in the unit cell is $Fe_{16}O_{24}$ and each Fe site is contained four times, therefore, the proportion of tetrahedral sites in the unit cell is 25%.

In 2004, our group synthesized single phase of ε-Fe_2O_3 by chemical synthesis method combination of reverse micelle method and sol-gel method [6]. First of all, reverse micelle containing iron nitrate aqueous solution and barium nitrate aqueous solution, and reverse micelle containing aqueous ammonia solution are prepared in octane and butanol solvent. Then, by mixing these reverse micelle, hydroxide nanoparticles were prepared. By adding tetraethyl orthosilicate, hydroxide nanoparticles were covered with glass. After removing the solvent, the precipitate was dried, and was sintered in air. Sintering at 900 °C and 1100 °C, γ-Fe_2O_3 and α-Fe_2O_3 were obtained respectively, however, at 1000 °C, ε-Fe_2O_3 was obtained. Transmission electron microscope (TEM) showed that this material was rod-shaped nanoparticles. Fourier transformation of the HRTEM images showed that the rod direction of this material is the a-axis direction. Our group Sakurai et al. reported the precise atomic coordinates by Rietveld analysis of the X-ray diffraction pattern in 2005 [40]. The space group is an orthorhombic $Pna2_1$, and the lattice constants are $a = 5.1019(3)$ Å, $b = 8.7807(6)$ Å, $c = 9.4661(5)$ Å.

While γ-Fe_2O_3, and α-Fe_2O_3 are abundant in nature, β-Fe_2O_3 and ε-Fe_2O_3 are obtained only in the laboratory. In 2009, Sakurai et al. reported the mechanism of generation the ε-Fe_2O_3 [41]. γ-Fe_2O_3, ε-Fe_2O_3, β-Fe_2O_3, and α-Fe_2O_3 can be prepared by synthesis method using mesoporous silica with only changing the sintering temperature. Synthesis is done as follows. First of all, mesoporous silica with small holes penetrated

iron sulfate or ferrocenecarbaldehyde was prepared. They were sintered at different temperatures in the air. As the sintering temperature was increased, γ-Fe$_2$O$_3$, ε-Fe$_2$O$_3$, β-Fe$_2$O$_3$, and α-Fe$_2$O$_3$ were obtained in turn. In this report, particle size threshold of phase transition were existed, i.e., the transition from γ-Fe$_2$O$_3$ to ε-Fe$_2$O$_3$ is about 8 nm, from ε-Fe$_2$O$_3$ to β-Fe$_2$O$_3$ is about 30 nm, and from β-Fe$_2$O$_3$ to α-Fe$_2$O$_3$ is about 50 nm in the synthesis method using iron sulfate. The surface energy play an important role in those transition. When describing the bulk part and the surface part separately, the Gibbs free energy (G) can be written as follows.

$$G(i) = G_B(i) + \left(\frac{6V_m}{d}\right) G_S(i)$$

Where, G_B is bulk Gibbs free energy, G_S is surface Gibbs free energy, V_m is molar volume, d is diameter, and i represents each phase (α, β, γ, and ε). If the Gibbs free energy of each phase satisfied following relationships, the particle size dependency of Gibbs free energy can be describe as Figure 1-5.

$$G_B(\gamma) > G_B(\varepsilon) > G_B(\beta) > G_B(\alpha)$$

and

$$G_S(\gamma) < G_S(\varepsilon) < G_S(\beta) < G_S(\alpha)$$

Figure 1-5 showed that each phase has moderate particle size in order to obtain those phases. This results are consistent with the fact that ε-Fe$_2$O$_3$ was only obtained as nanoscale.

ε-Fe$_2$O$_3$ have received increased attention due to interesting properties [42-52]. For example, ε-Fe$_2$O$_3$ exhibits huge coercive field value over 25 kOe and saturation magnetization value 15 emu/g (Figure 1-6). The origin of magnetism of ε-Fe$_2$O$_3$ is considered as follows. Among the four Fe sites, A site and D site have negative sublattice magnetization, and B site and C site have positive sublattice magnetization.

Because the value of sublattice magnetization at D site is slightly smaller than the other sites, the positive magnetization of the B site and the C site cannot be canceled out by the negative magnetization of the A site and the D site in total. Therefore, ε-Fe_2O_3 exhibits ferrimagnetism. In addition, ε-Fe_2O_3 can be absorbed the high frequency millimeter wave such as 182 GHz, since ε-Fe_2O_3 is insulator and exhibits huge coercive field value [43].

Fe^{3+} ions of ε-Fe_2O_3 can be substituted by other trivalent cations, i.e., Al^{3+}, Ga^{3+}, In^{3+}, Rh^{3+} and so on [7, 53-64]. Al^{3+} ion and Ga^{3+} ion can selectively replace the D site (Figure 1-7). By substitution of Al^{3+} (d^0 $S = 0$) or Ga^{3+} (d^{10} $S = 0$), the sublattice magnetization at D site decreases, and the saturation magnetization values of ε-Fe_2O_3 increase. On the other hand, the coercive field values decreases as the amount of Al^{3+} ion or Ga^{3+} ion substitution increases. Rh^{3+} can selectively replace the C site. By Rh-substitution, hybridization of the orbit becomes stronger. Therefore, the coercive field values are increased. Since the frequency of the electromagnetic waves absorption is related to coercive field values, this value can be controlled by metal substitution from 35 GHz to 222 GHz. As shown in these examples, various physical properties can be controlled by metal substitution of ε-Fe_2O_3.

1.3. Transparent magnets

Typical magnetic materials show deep color. For example, metal magnets reflect visible light and show silver color. On the other hand, it is considered that the magnetic materials exhibiting light-color or transparency can widen the usage of magnets. There are several reports on transparent magnetic materials [65-67]. Since ferrites are magnetic material and have a band gap, they are good candidate for

transparency magnets. It is known that a ferrite having a large particle size shows a deep color due to scattering of light, however, if the particle size is reduced, scattering of visible light can be suppressed, and the color becomes lighter. In 1992, R. F. Ziolo et al. reported that composite material which contain γ-Fe_2O_3 nanoparticles and polymer exhibit highly transparency [67].

1.4. Objective

The objective of this theses is to investigate the color of epsilon iron oxide. The origin of the color was clarified by first-principles calculations and UV-vis absorption measurement. Furthermore, the effects on optical absorption by metal-substitution were investigated. Al- and Ga-substituted epsilon iron oxides were investigated using first-principles calculations and UV-vis spectra.
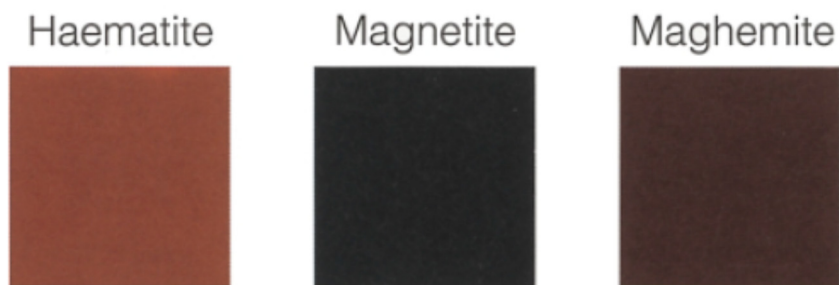
Figure 1-1. The color of iron oxides. Left is α-Fe_2O_3, center is Fe_3O_4, and right is γ-Fe_2O_3 [14].

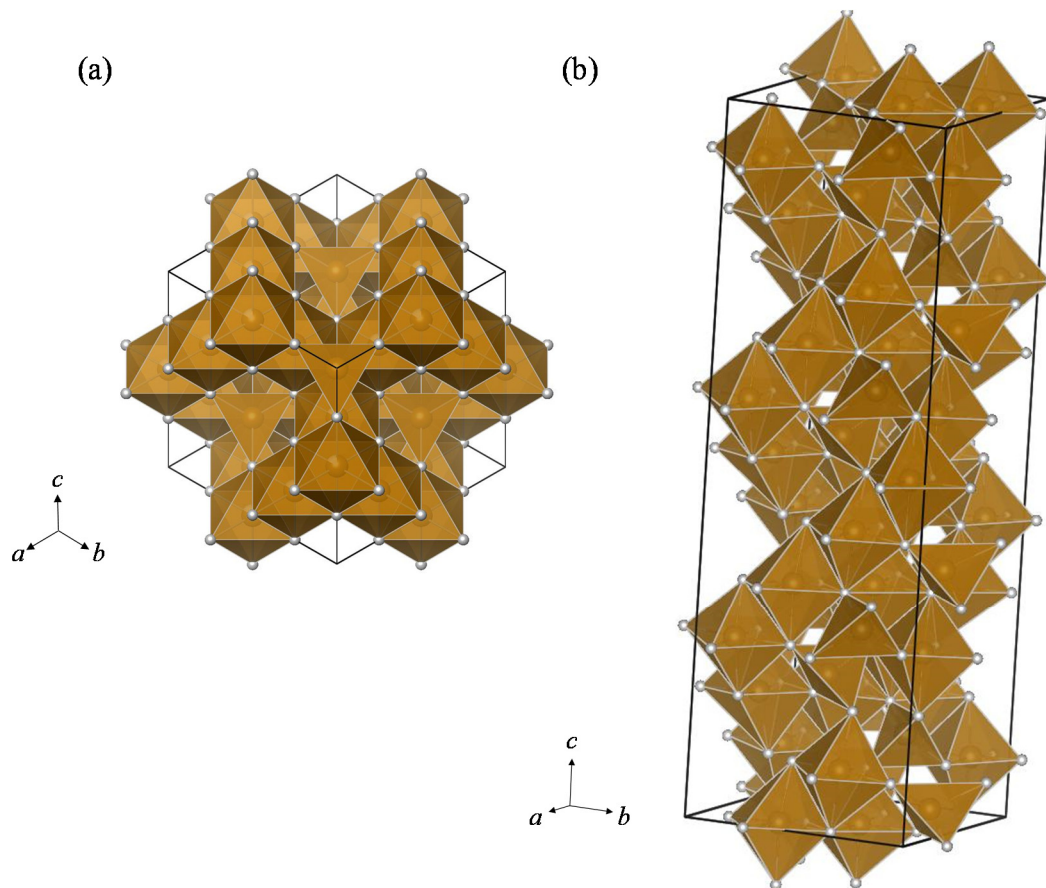Reproduced by permission from John Wily & Sons, Inc.: R. M. Cornell, and U. Schwertmann, Wiley-VCH Verlag GmbH & Co. KGaA (2003)

Figure 1-2. Crystal structure of γ-Fe₂O₃. (a) Cubic crystal structure and (b) tetragonal crystal structure [24, 25].

Reproduce with permission from Springer, C. Pecharromán, T. González-Carreño, J. E. Iglesias, **Phys. Chem. Minerals**, *22*, 21-29 (1995). Copyright 1995, Springer-Verlag.
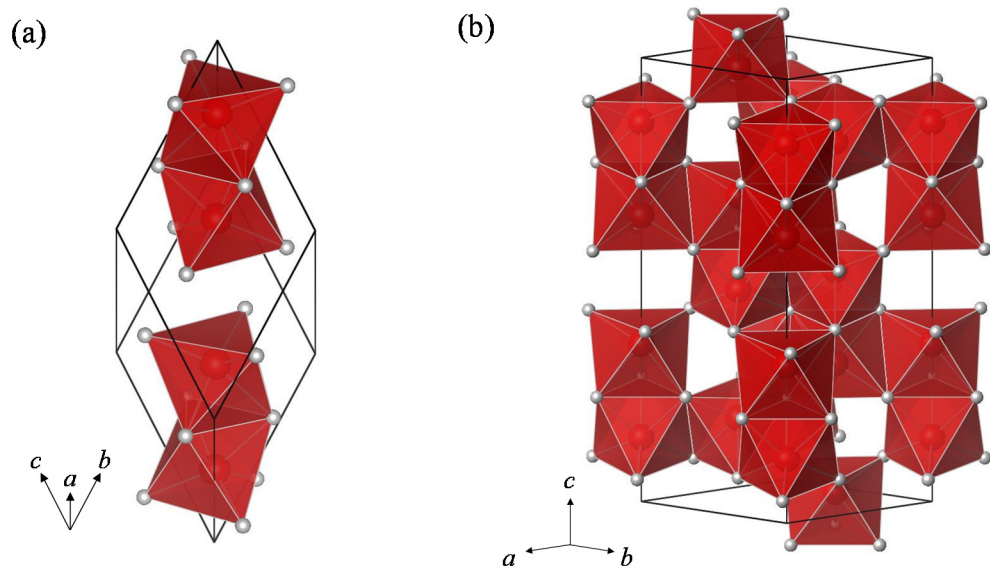
Figure 1-3. Crystal structure of α-Fe$_2$O$_3$. (a) Rhombohedral crystal structure and (b) hexagonal crystal structure [29].

Reprinted with permission from L. Pauling, and S. B. Hendricks, ***J. Am. Chem. Soc.***, *47*, 3, 781-90 (1925). Copyright 1925 American Chemical Society.

Figure 1-4. Crystal structure of ε-Fe₂O₃. Blue octahedral, green octahedral, orange octahedral, red tetrahedral, and gray balls indicate FeA site, FeB site, FeC site, FeD site, and oxygen atom, respectively [39].

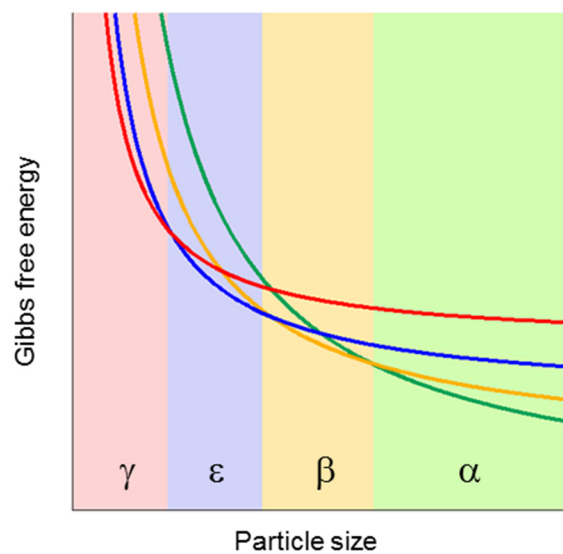**Figure 1-5.** Schematic illustration of phase stabilities among Fe$_2$O$_3$. Red, blue, yellow, and green lines indicate Gibbs free energy of γ-Fe$_2$O$_3$, ε-Fe$_2$O$_3$, β-Fe$_2$O$_3$, and α-Fe$_2$O$_3$, respectively [41].

Reprinted with permission from S. Sakurai, A. Namai, K. Hashimoto, and S. Ohkoshi, *J. Am. Chem. Soc.*, *131*, 18299-18303 (2009). Copyright 2009 American Chemical Society.
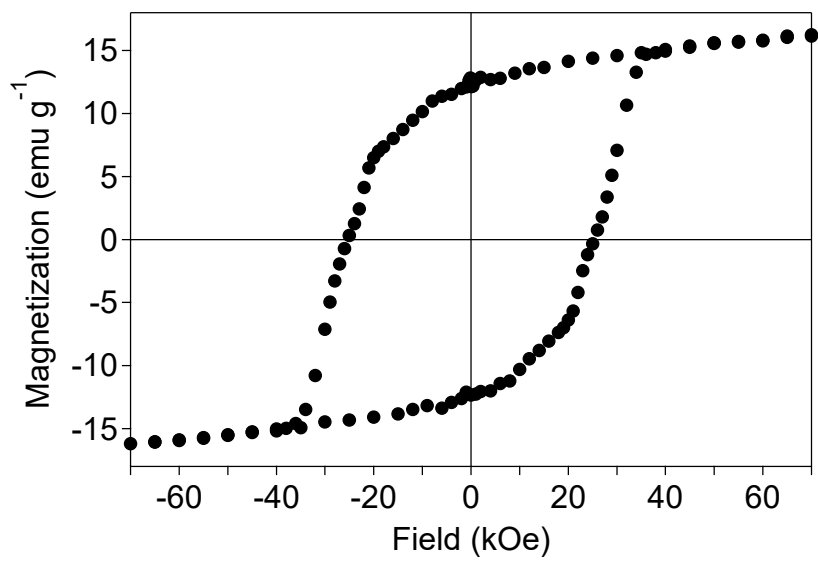
Figure 1-6. Magnetic hysteresis loop of ε-Fe$_2$O$_3$ [8].
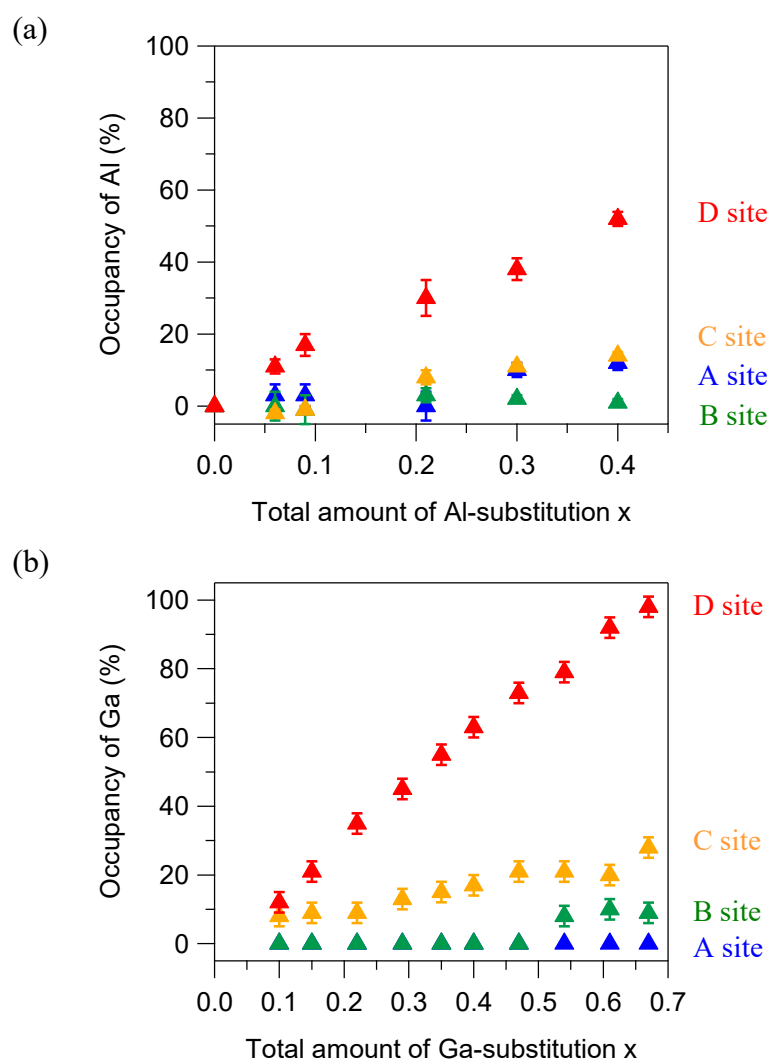
Figure 1-7. Amount of (a) Al- and (b) Ga-substitution dependency for occupancy of each cation sites in ε-Al$_x$Fe$_{2-x}$O$_3$ or ε-Ga$_x$Fe$_{2-x}$O$_3$. Blue, green, orange, and red marks indicate the occupancies of A, B, C, and D sites, respectively [43, 57].

Reprinted with permission from A. Namai, S. Sakurai, M. Nakajima, T. Suemoto, K. Matsumoto, M. Goto, S. Sasaki, S. Ohkoshi, *J. Am. Chem. Soc.*, *131*, 1170–1173 (2009). Copyright 2009 American Chemical Society.

Reproduced by permission from John Wily & Sons, Inc.: S. Ohkoshi, S. Kuroki, S. Sakurai, K. Matsumoto, K. Sato, and S. Sasaki, *Angew. Chem. Int. Ed.*, *46*, 8392-8395 (2007). Copyright 2007, WILEY-VCH Verlag GmbH & Co. KGaA, Weinheim.

Chapter 2 First-principles calculations and optical measurement of ε-Fe$_2$O$_3$

本章については特許申請のため、また、雑誌等で刊行予定のため、非公開。

Chapter 3 Al-substitution effect on epsilon iron oxide for optical absorption

本章については特許申請のため、また、雑誌等で刊行予定のため、非公開。

Chapter 4 Ga-substitution effect on epsilon iron oxide for optical absorption

本章については特許申請のため、また、雑誌等で刊行予定のため、非公開。

Chapter 5 Summary and Prospective

In this study, I clarified the optical absorption properties of epsilon iron oxide using first-principles calculations and UV-vis spectra.

In chapter 2, first-principles calculations of ε-Fe_2O_3 showed that ε-Fe_2O_3 has a wide band gaps and the absorption around 560 nm assigned transitions from O sites neighboring FeD site to FeC site. Furthermore, highly dispersed polymer solution of ε-Fe_2O_3 was prepared. The UV-vis spectrum of this solution confirmed the calculation results, and these results revealed that ε-Fe_2O_3 is a light-colored magnetic material.

In chapter 3, first-principles calculations of ε-$Al_{0.5}Fe_{1.5}O_3$ was performed, in order to investigate the effect of Al-substitution for optical absorption. First-principles calculations are conducted using the crystal structure with Fe D site selectively substituted by Al^{3+} ion. The first-principles calculations suggested that the band gaps of ε-Fe_2O_3 enlarged by Al-substitution because the absorption around 560 nm in ε-Fe_2O_3 disappeared by Al-substitution. Furthermore, UV-vis spectra of ε-$Al_xFe_{2-x}O_3$ ($x = 0.48$, and 0.66) confirmed the calculation results, and clarified that Al-substitution lightens the color of ε-Fe_2O_3.

In chapter 4, Ga-substitution effect on ε-Fe_2O_3 for optical absorption was investigated. Ga-substitution also lightens the color of ε-Fe_2O_3, with the same mechanism of Al-substitution.

In this thesis, it is clarified that the color of ε-Fe_2O_3 magnetic material is light, and furthermore, the color becomes lighter by Al- or Ga-substitution. For the further development of even lighter-colored magnets, it is important to design the materials using first-principles calculations because first-principles calculations can predict the

suitable atoms and substitution sites for develop light-colored magnets.

References

[1] P. A. Cox

The Electronic Structure and Chemistry of Solids

Oxford University Press (1987).

[2] M. Imada, A Fujimori, and Y. Tokura

Metal-insulator transitions

Rev. Modern Phys., *70*, 4, 1039-1263 (1998).

[3] H. Kronmüller and S. Parkin

Hand book of Magnetism and Advanced Magnetic Materials

Wiley (2007).

[4] J. M. D. Coey

Magnetism and Magnetic Materials

Cambridge University Press (2010).

[5] D. J. Craik

Magnetic Oxides

Wiley-Interscience publication (1975).

[6] J. Jin, S. Ohkoshi, K. Hashimoto

Giant coercive field of nanometer-size iron oxide

Adv. Mater., *16*, 48–51 (2004).

[7] S. Ohkoshi, H. Tokoro

Hard magnetic ferrite: ε-Fe_2O_3

Bull. Chem. Soc. Jpn., *86*, 897–907 (2013).

[8] S. Ohkoshi, A. Namai, T. Yamaoka, M. Yoshikiyo, K. Imoto, T. Nasu, S. Anan, Y. Umeta, K. Nakagawa, and H. Tokoro

Mesoscopic bar magnet based on ε-Fe$_2$O$_3$ hard ferrite

Sci. Rep., *6*, 27212/1-10 (2016).

[9] S. Ohkoshi, Y. Tsunobuchi, T. Matsuda, K. Hashimoto, A. Namai, F. Hakoe, and H. Tokoro

Synthesis of a metal oxide with a room-temperature photoreversible phase transition

Nat. Chem., *2*, 539-545 (2010).

[10] H. Tokoro, M. Yoshikiyo, K. Imoto, A. Namai, T. Nasu, K. Nakagawa, N. Ozaki, F. Hakoe, K. Tanaka, K. Chiba, R. Makiura, K. Prassides, and S. Ohkoshi

External stimulation-controllable heat-storage ceramics

Nat. Commun., *6*, 7037/1-8 (2015).

[11] T. Nasu, H. Tokoro, K. Tanaka, F. Hakoe, A. Namai, and S. Ohkoshi

Sol-gel synthesis of nanosized λ-Ti$_3$O$_5$ crystals

Mater. Sci. and Eng., *54*, 012008 (2014).

[12] K. Tanaka, T. Nasu, Y. Miyamoto, N. Ozaki, S. Tanaka, T. Nagata, F. Hakoe, M. Yoshikiyo, K. Nakagwa, Y. Umeta, K. Imoto, H. Tokoro, A. Namai, and S. Ohkoshi

Structural phase transition between, γ-Ti$_3$O$_5$ and δ-Ti$_3$O$_5$ by breaking of one-dimensionally conducting pathway

Cryst. Growth Des., *15*, 654 (2015).

[13] R. Valenzuela

Magnetic ceramics

Cambridge University Press (1994).

[14] R. M. Cornell, U. Schwertmann

The Iron Oxides: Structure, Properties, Reactions, Occurences and Uses

Wiley-VCH Verlag GmbH & Co. KGaA (2003).

[15] B. Gilbert, C. Frandsen, E. R. Maxey, D. M. Sherman

Band-gap measurements of bulk and nanoscale hematite by soft x-ray spectroscopy

Phys. Rev. B, *79*, 035108 (2009).

[16] L. Machala, J. Tuček, R. Zbořil

Polymorphous transformations of nanometric iron(III) oxide: A review

Chem. Mater., *23*, 3255–3272 (2011).

[17] M. I. Litter, M. A. Blesa

Photodissolution of iron oxides. IV. A comparative study on the photodissolution of hematite, magnetite, and maghemite in EDTA media

Can. J. Chem., *70*, 2502-2510 (1992).

[18] R. Grau-Crespo, A. Y. Al-Baitai, I. Saadoune, N. H. D. Leeuw

Vacancy ordering and electronic structure of γ-Fe_2O_3 (maghemite) : a theoretical investigation

J. Phys.: Condens. Mater., *22*, 255401 (2010).

[19] S. Chikazumi

Physics of Ferromagnetism

Oxford University Press, New York (1997).

[20] W. H. Bragg

The structure of magnetite and the spinels

Nature, *95*, 561 (1915).

[21] S. Nishikawa

Structure of some crystals of spinel group

Proc. Math. Phys. Soc. Tokyo, **8**, 199-209 (1915).

[22] R. J. Hill, J. R. Craig, and G. V. Gibbs

Systematics of the spinel structure type

Phys. Chem. Minerals, *4*, 315-339 (1979).

[23] E. J. W. Verwey

Electronic conduction of magnetite (Fe_3O_4) and its transition point at low temperatures

Nature, *144*, 327-238 (1939).

[24] C. Pecharromán, T. González-Carreño, J. E. Iglesias

The Infrared dielectric properties of maghemite, γ-Fe_2O_3, from reflectance measurement on pressed powders

Phys. Chem. Minerals, *22*, 21-29 (1995).

[25] J.-E. Jorgensen, L. Mosegaard, L. E. Thomsen, T. R. Jensen, J. C. Hanson

Formation of γ-Fe_2O_3 nanoparticles and vacancy ordering: An in situ X-ray powder diffraction study

J. Solid State Chem., *180*, 180-185 (2007).

[26] E. Solano, C. Frontera, T. Puig, X. Obradors, S. Ricart and J. Ros

Neutron and X-ray diffraction study of ferrite nanocrystals obtained by microwave-assisted growth. A structural comparison with the thermal synthetic route

J. Appl. Cryst., *47*, 414-420 (2014).

[27] A. N. Shmakov, G. N. Kryukova, S. V. Tsyvulya, A. L. Chuvilin and L. P. Solovyeva

Vacancy ordering in γ-Fe_2O_3 : Synchrotron X-ray powder diffraction and high-resolution electron microscopy studies

J. Appl. Cryst., *28*, 141-145 (1995).

[28] C. Greaves

A powder neutron diffraction investigation of vacancy ordering and covalence in γ-Fe_2O_3

J. Solid, State, Chem., *49*, 325-333 (1983).

[29] L. Pauling, and S. B. Hendricks

The crystal structures of hematite and corundum

J. Am. Chem. Soc., *47*, 3, 781-90 (1925).

[30] L. W. Finger, and R. M. Hazen

Crystal structure and isothermal compression of Fe_2O_3, Cr_2O_3, and V_2O_3 to 50 kbars

J. Appl Phys., *51*, 5362-5367 (1980).

[31] R. L. Blake and R. E Hessevick

Refinement of the hematite structure

Amer. Mineral., *51*, 123-129 (1966)

[32] E. N. Maslen, V. A. Streltsov, N. R. Streltsova, and N. Ishizawa

Synchrotron X-ray study of the electron density in α-Fe_2O_3

Acta Cryst., *B50*, 435-441 (1994).

[33] J. O. Artman, J. C. Murphy, and S. Goner

Magnetic anisotropy in antiferromagnetic corundum-type sesquioxides

Phys. Rev., *138*, A912 (1965).

[34] F. J. Morin

Magnetic susceptibility of αFe_2O_3 and αFe_2O_3 with added titanium

Phys. Rev., *78*, 819 (1950).

[35] I. Dzyaloshinsky

A thermodynamic theory of "weak" ferromagnetism of antiferromagnetics

J. Phys. Chem. Solids, *4*, 241-255 (1958).

[36] T. Moriya

New mechanism of anisotropic superexchange interaction

Phys. Rev. Lett., *4*, 228-230 (1960).

[37] H. Forestier and G. Guiot-Guillain

Une nouvelle variété ferromagnétique de sesquioxyde de fer

C. R. Acad. Sci. (Paris), *199*, 720 (1934).

[38] V. R. Schrader, and G. Büttner

Eine neue eisen(III)-oxidphase: ε-Fe_2O_3

Z. anorg. Allg. Chemie. Bd., *320*, 220-234 (1963).

[39] E. Tronc, C. Chanéac, and J. P. Jolivet

Structural and magnetic characterization of ε-Fe_2O_3

J. Solid State Chem., *139,* 93-104 (1998).

[40] S. Sakurai, J. Jin, K. Hashimoto, and S. Ohkoshi

Reorientation phenomenon in a magnetic phase of ε-Fe_2O_3 nanocrystal

J. Phys. Soc. Jap., *74*, 1946-1949 (2005).

[41] S. Sakurai, A. Namai, K. Hashimoto, and S. Ohkoshi

First observation of phase transformation of all four Fe_2O_3 phases ($\gamma \rightarrow \varepsilon \rightarrow \beta \rightarrow \alpha$)

J. Am. Chem. Soc., *131*, 18299-18303 (2009).

[42] J. Tuček, R. Zbořil, A. Namai, and S. Ohkoshi

ε-Fe$_2$O$_3$: An advanced nanomaterial exhibiting giant coercive field, millimeter-wave ferromagnetic resonance, and magnetoelectric coupling

Chem. Mater., *22*, 6483–6505 (2010).

[43] A. Namai, S. Sakurai, M. Nakajima, T. Suemoto, K. Matsumoto, M. Goto, S. Sasaki, S. Ohkoshi

Synthesis of an electromagnetic wave absorber for high-speed wireless communication

J. Am. Chem. Soc., *131*, 1170–1173 (2009).

[44] E. Tronc, C. Chanéac, J. P. Jolivet, J. M. Grenèche

Spin collinearity and thermal disorder in ε-Fe$_2$O$_3$

J. Appl. Phys., *98*, 053901 (2005).

[45] Y.-C. Tseng, N. M. Souza-Neto, D. Haskel, M. Gich, C. Frontera, A. Roig, M. Veenendaal, J. Nogués

Nonzero orbital moment in high coercivity ε-Fe$_2$O$_3$ and low-temperature collapse of the magnetocrystalline anisotropy

Phys. Rev. B, *79*, 094404 (2009).

[46] D. A. Balaev, I. S. Poperechny, A. A. Krasikov, K. A. Shaikhutdinov, A. A. Dubrovskiy, S. I. Popkov, A. D. Balaev, S. S. Yakushkin, G. A. Bukhtiyarova, O. N. Martyanov, Y. L. Raikher

Dynamic magnetization of ε-Fe$_2$O$_3$, in pulse field: Evidence of surface effect

J. Appl. Phys., *117* 063908 (2015).

[47] J. Kohout, P. Brázda, K. Závěta, D. Kubániová, T. Kmječ, L. Kubíčková, M. Klementová, E. Šantavá, A. Lančok

The magnetic transition in ε-Fe_2O_3 nanoparticles: Magnetic properties and hyperfine interactions from Mössbauer spectroscopy

J. Appl. Phys., *117*, 17D505 (2015).

[48] J. López-Sánchez, A. Serrano, A. Del Campo, M. Abuín, O. Rodríguez de la Fuente, N. Carmona

Sol-Gel synthesis and micro-raman characterization of ε-Fe_2O_3 micro- and nanoparticles

Chem. Mater., *28*, 511−518 (2016).

[49] S. Lee, H. Xu

Size-dependent phase map and phase transformation kinetics for nanometric iron(III) Oxides ($\gamma \rightarrow \varepsilon \rightarrow \alpha$ Pathway)

J. Phys. Chem. C, *120*, 13316−13322 (2016).

[50] A. A. Dubrovskiy, D. A. Balaev, K. A. Shykhutdinov, O. A. Bayukov, O. N. Pletnev, S. S. Yakushkin, G. A. Bukhtiyarova, and O. N. Martyanov

Size effects in the magnetic properties of ε-Fe_2O_3 nanoparticles

J. Appl. Phys., *118*, 213901 (2015).

[51] P. Brázda, E. Večerníková, E. Pližingrová, A. Lančok, and D. Nižňanský

Thermal stability of nanocrystalline ε-Fe_2O_3

J. Therm. Ananl. Calorim., *117*, 85-91 (2014).

[52] M. Yoshikiyo, K. Yamada, A. Namai, and S. Ohkoshi

Study of the electronic structure and magnetic properties of ε-Fe_2O_3 by first-principles calculation and molecular orbital calculations

J. Phys. Chem. C, *116*, 8688–8691 (2012).

[53] M. N. Afsar, Z. Li, K. A. Korolev, A. Namai, and S. Ohkoshi

Magneto absorption measurements of nano-size ε-Al$_x$Fe$_{2-x}$O$_3$ powder materials at millimeter wavelengths

J. Appl. Phys., *109*, 07E316 (2011).

[54] M. N. Afsar, Z. Li, K. A. Korolev, A. Namai, and S. Ohkoshi

A millimeter-wave tunable electromagnetic absorber based on ε-Al$_x$Fe$_{2-x}$O$_3$ Nanomagnets

IEEE Trans. Mag., *47*, 333-336 (2011).

[55] M. N. Afsar, K. A. Korolev, A. Namai, and S. Ohkoshi

Millimeter-Wave ferromagnetic absorption of epsilon aluminum iron oxide nano ferrites

IEEE Trans. Mag., *47*, 2588-2591 (2011).

[56] M. N. Afsar, Fellow IEEE, K. A. Korolev, A. Namai, and S. Ohkoshi

Measurements of complex magnetic permeability of nano-Size ε-Al$_x$Fe$_{2-x}$O$_3$ powder materials at microwave and millimeter wavelengths

IEEE Trans. Mag., *48*, 2769-2772 (2012).

[57] S. Ohkoshi, S. Kuroki, S. Sakurai, K. Matsumoto, K. Sato, and S. Sasaki

A millimeter-wave absorber based on gallium-substituted ε-iron oxide nanomagnets

Angew. Chem. Int. Ed., *46*, 8392-8395 (2007).

[58] A. Namai, S. Kurahashi, H. Hachiya, K. Tomita, S. Sakurai, K Matatsumoto, T. Goto, and S. Ohkoshi

High magnetic permeability of ε-Ga$_x$Fe$_{2-x}$O$_3$ magnets in the millimeter wave region

J. Appl. Phys., *107*, 09A955 (2010).

[59] S. Sakurai, S. Kuroki, H. Tokoro, K. Hashimoto, and S. Ohkoshi

Synthesis, crystal structure, and magnetic properties of ε-In$_x$Fe$_{2-x}$O$_3$ nanorod-shaped magnets

Adv, Func. Mater., *17*, 2278-2282 (2007).

[60] K. Yamada, H. Tokoro, M. Yoshikiyo, T. Yroinaga, A. Namai, and S. Ohkoshi

The phase transition of ε-In$_x$Fe$_{2-x}$O$_3$ nanomagnets with a large thermal hysteresis loop

J. Appl. Phys., *111*, 07B506 (2012).

[61] M. Yoshikiyo, A. Namai, M. Nakajima, K. Yamaguchi, T. Suemoto, and S. Ohkoshi

High-frequency millimeter wave absorption of indium-substituted ε-Fe$_2$O$_3$ spherical nanoparticles

J. Appl. Phys., *115*, 172613 (2014).

[62] A. Namai, M. Yoshikiyo, K. Yamada, S. Sakurai, T. Goto, T. Yoshida, T. Miyazaki, M. Nakajima, T. Suemoto, H. Tokoro, S. Ohkoshi

Hard magnetic ferrite with a gigantic coercivity and high frequency millimetre wave rotation

Nat. Commun., *3*, 1035 (2012).

[63] A. Namai, M. Yoshikiyo, S. Umeda, T. Yoshida, T. Miyazaki, M. Nakajima, K. Yamaguchi, T. Suemoto, and S. Ohkoshi

The synthsis of rhodium substituted ε-iron oxide exhibiting super high frequency natural resonance

J. Mater. Chem. C, *1*, 5200-5206 (2013).

[64] S. Ohkoshi, A. Namai, M. Yoshikiyo, K. Imoto, K. Tamazaki, K. Matsuno, O. Inoue, T. Ide, K. Masada, M. Goto, T. Goto, T. Yoshida, and T. Miyazaki

Multimetal-substituted epsilon-Iron oxide ε-$Ga_{0.31}Ti_{0.05}Co_{0.05}Fe_{1.59}O_3$ for next-generation magnetic recording tape in the big-data era

Angew. Chem. Int. Ed., *55*, 11403-11406 (2016).

[65] Y. Matsumoto, M. Murakami, T. Shono, T. Hasegawa, T. Fukumura, M. Kawasaki, P. Ahmet, T. Chikyow, S. Koshihara, H. Koinuma

Room-temperature ferromagnetism in transparent transition metal-doped titanium dioxide

Science, *291*, 854-856 (2001).

[66] T. Fukuyama, H. Toyosaki, K. Ueno, M. Nakano, and M. Kawasaki

Role of charge carriers for ferromagnetism in cobalt-doped rutile TiO_2

New J. Phys., *10*, 055018 (2008).

[67] R. F. Ziolo, E. P. Giannelis, B. A. Weinstein, M. P. O'Horo, B. N. Ganguly, V. Mehrotra, M. W. Russell, D. R. Huffman

Matrix-mediated synthesis of nanocrystalline γ-Fe_2O_3: A new optically transparent magnetic material

Science, *257*, 219–223 (1992).

[68] S. Ohkoshi, A. Namai, K. Imoto, M. Yoshikiyo, W. Tarora, K. Nakagawa, M. Komine, Y. Miyamoto, T. Nasu, S. Oka, H. Tokoro

Nanometer-size hard magnetic ferrite exhibiting high optical-transparency and optical-magnetoelectric effect

Sci. Rep., *5*, 14414 (2015).

[69] G. Kresse, J. Hafner

Ab initio molecular dynamics for open-shell transition metals

Phys. Rev. B, *48*, 13115-13118 (1993).

[70] G. Kresse, and J. Hafner

Ab initio molecular dynamics for liquid metals

Phys. Rev. B, *47*, 558-561 (1993)

[71] G. Kresse, J. Furthmüller

Efficient iterative schemes for *ab initio* total-energy calculations using a plane-wave basis set

Phys. Rev. B, *54*, 11169-11186 (1996).

[72] G. Kresse, J. Furthmüller

Efficiency of ab-initio total energy calculations for metals and semiconductors using a plane-wave basis set

Comp. Mater. Sci., *6*, 15-50 (1996).

[73] M. Gajdoš, K. Hummer, G. Kresse, J. Futhmüller, and F. Bechstedt

Linear optical properties in the projector-augmented wave methodology

Phys. Rev. B, *73*, 045112/1-9 (2006).

[74] S. Ohkoshi, et al., JP patent 2015-008160

[75] T. Nasu, M. Yoshikiyo, H. Tokoro, A. Namai, and S. Ohkoshi

First-principles calculations and optical absorption spectrum of a light-colored Al-substituted epsilon iron oxide magnet

Eur. J. Inorg. Chem, *3*, 531-534 (2017).

List of papers related to the thesis

(1) "Nanometer-size hard magnetic ferrite exhibiting high optical transparency and nonlinear optical-magnetoelectric effect"

S. Ohkoshi, A. Namai, K. Imoto, M. Yoshikiyo, W. Tarora, K. Nakagawa, M. Komine, Y. Miyamoto, T. Nasu, S. Oka, H. Tokoro,

Scientific Reports, *5*, 14414 (2015).

A part of this paper corresponds to Chapter 2.

(2) "First-principles calculations and optical absorption spectrum of a light-colored Al-substituted epsilon iron oxide magnet"

T. Nasu, M. Yoshikiyo, H. Tokoro, A. Namai, and S. Ohkoshi,

European Journal of Inorganic Chemistry, *3*, 531-534 (2017).

This paper corresponds to Chapter 3.

Acknowledgement

I would like to express my great gratitude to my supervisor, Professor Shin-ichi Ohkoshi for giving the fascinating research theme and environment. Thanks to accurate advices on the discussion, I was able to carry out my research in this laboratory. Furthermore, I learned various important things from him. Again, I really appreciate him in all aspects of my reserch.

I would like to thank Associate Professor Hiroko Tokoro in University of Tsukuba. I learned experiment and various things about research from her.

I would like to thank Project Assistant Professor Marie Yoshikiyo. She taught me about the first-principles calculations, and how to write the paper. I appreciate the daily discussions with her. I would like to thank Assistant Professor Asuka Namai for useful advice and discussions. Furthermore, samples were supplied by them.

I would like to thank Assistant Professor Koji Nakabayashi, Project Assistant Professor Kosuke Nakagawa and Project Assistant Professor Kenta Imoto for a lot of useful advice and discussions.

I woule like to thank Dr. Kouji Chiba of Ryoka Systems Inc. for valuable discussion and for teaching me about the first-principles calculations.

I am grateful to Mr. Yasutomi Kakegawa, Mr. Shigeru Ohtsuka, and Mr. Hideo Tsunakawa for collecting transmittance electron microscope and scanning electron microscope images.

I apprceate the MERIT program for financial support and significant programs. I acknowledge vice-supervisor, Prof. Atsuo Yamada and MERIT members for useful discussions. I appreciate Dr. Tohru Kawamoto, Dr. Akira Takahashi and all their group